Miner Deposita (2006) 41:785–801
DOI 10.1007/s00126-006-0099-x

ARTICLE

Early Cretaceous U–Pb zircon ages for the Copiapó plutonic complex and implications for the IOCG mineralization at Candelaria, Atacama Region, Chile

Robert Marschik · Frank Söllner

Received: 8 May 2006 / Accepted: 11 September 2006 / Published online: 20 October 2006

Abstract Four of the major plutons in the vicinity of the Candelaria mine (470 Mt at 0.95% Cu, 0.22 g/t Au, 3.1 g/t Ag) and a dike–sill system exposed in the Candelaria open pit have been dated with the U–Pb zircon method. The new geochronological data indicate that dacite magmatism around 123 Ma preceded the crystallization of hornblende diorite (Khd) at 118±1 Ma, quartz–monzonite porphyry (Kqm) at 116.3±0.4 Ma, monzodiorite (Kmd) at 115.5±0.4 Ma, and tonalite (Kt) at 110.7±0.4 Ma. The new ages of the plutons are consistent with field relationships regarding the relative timing of emplacement. Plutonism temporally overlaps with the iron oxide Cu–Au mineralization (Re–Os molybdenite ages at ~115 Ma) and silicate alteration (ages mainly from 114 to 116 and 110 to 112 Ma) in the Candelaria–Punta del Cobre district. The dated dacite porphyry and hornblende diorite intrusions preceded the ore formation. A genetic link of the metallic mineralization with the quartz–monzonite porphyry and/or the monzodiorite is likely. Both of these metaluminous, shoshonitic (high-K) intrusions could have provided energy and contributed fluids, metals, and sulfur to the hydrothermal system that caused the iron oxide Cu–Au mineralization. The age of the tonalite at 110.7 Ma falls in the same range as the late alteration at 110 to 112 Ma. Tonalite emplacement may have sustained existing or driven newly developed hydrothermal cells that caused this late alteration or modified $^{40}Ar/^{39}Ar$ and K/Ar systematic in some areas.

Editorial handling: A. Boyce

R. Marschik (✉) · F. Söllner
Department of Earth and Environmental Sciences,
Ludwig-Maximilians-Universität,
Luisenstrasse 37,
80333 Munich, Germany
e-mail: marschik@lmu.de

Keywords Candelaria–Punta del Cobre · Chile · IOCG deposits · U–Pb zircon dating

Introduction

Magmas that formed the plutonic rocks south of Copiapó, northern Chile (Copiapó plutonic complex, e.g., Marschik et al. 2003a) are heat and potential fluid, metal, and sulfur source for the Early Cretaceous (~115 Ma) hydrothermal iron oxide-rich Cu–Au mineralization in the Candelaria–Punta del Cobre district (e.g., Marschik et al. 1997; Marschik and Fontboté 2001a; Mathur et al. 2002). Petrographic studies on the rocks of the Copiapó plutonic complex date back to the early 1960s (Tilling 1962, 1963a, 1976). Geochemical and petrogenetic isotope geochemical studies were carried out by McNutt et al. (1975, 1979) and more recently by Mathur et al. (2002) and Marschik et al. (2003a). Previous geochronological studies, using K–Ar or $^{40}Ar/^{39}Ar$ isotope methods on igneous silicates from these plutons, provided a wide spectrum of ages ranging from 69 to 119 Ma (Farrar et al. 1970; Zentilli 1974; Arévalo 1994, 1995, 1999; Ullrich et al. 2001). They represent cooling ages or may record alteration or reheating events. The range of ages suggests a complex (hydro-)thermal history. U–Pb zircon ages provide reliable information on the time of crystallization due to a high closure temperature of about 900°C (Mezger and Krogstad 1997) and the fact that zircons are fairly resistant to post-magmatic (hydro)thermal alteration, although there is evidence from experiments for leaching of Pb, U, and Th from metamict zircon by hydrothermal fluids (Geisler et al. 2002). In this contribution, we present new U–Pb geochronological data on zircons from four units of the Copiapó plutonic complex and a dacite porphyry dike–sill system that cuts the

Candelaria ore body, and discuss the relevance of these data for the iron oxide Cu–Au ore genesis in the Candelaria–Punta del Cobre district.

Geologic context

The Late Jurassic–Early Cretaceous rocks of the Coastal Cordillera–Precordillera in the Atacama region represent a magmatic arc and an associated marine back-arc environment to the east (e.g., Marschik and Fontboté 2001b). The pre-Mesozoic basement is locally exposed in an approx. 25-km wide belt along the coast and in discontinuous outcrops in the Precordillera, east of Copiapó. Paleozoic rocks are mainly high-grade metamorphic rocks and granitoid intrusions (e.g., Brown 1991; Lucassen et al. 1999, 2002). The oldest reported protolith ages of about 1.46 to 1.21 Ga are for the Belén and Quebrada Choja supracrustal sequences in the Precordillera in northern Chile (Damm et al. 1990). Evidence for Late Archean basement components in the region comes from U–Pb upper intercept ages (2.69 to 2.78 Ga) for detrital zircons from Devonian metasedimentary rocks at Quebrada Las Animas near Chañaral (latitude 26°25′S; Berg and Baumann 1985). The strong discordance of the U–Pb data points suggests zircon growth around older cores, and the ages derived from these detrital zircons are interpreted to represent a metamorphic event at around 600 Ma (Berg and Baumann 1985). Further evidence for Neoproterozoic–Cambrian metamorphism ± magmatism between 525 and 500 Ma (Pampean Cycle) is provided by Sm–Nd isochrons for metamorphic rocks of northern Chile (e.g., Lucassen et al. 2000). Cambrian and Ordovician–Silurian plutonism occurred mostly in northwest Argentina (Damm et al. 1990, 1994), whereas Carboniferous to Permian intrusions are mainly exposed in the Chilean Coastal Cordillera and Precordillera (e.g., Damm et al. 1981; Brown 1991; Lucassen et al. 1999). Near Chañaral, a transition from alkaline S-type (mainly monzogranites and syenogranites) during Permian and Triassic towards calc-alkaline I-type magmatism (mainly tonalites and granodiorites) during the Late Jurassic to Early Cretaceous is recognized (Damm et al. 1981; Berg et al. 1983; Berg and Baumann 1985). The Permo-Triassic and Jurassic plutons intruded as laccoliths along low-angle extensional shear zones (Grocott et al. 1994; Grocott and Wilson 1997), whereas Early Cretaceous plutons emplaced as vertical sheets during arc-parallel lateral displacement along the Atacama Fault Zone (e.g., Scheuber and Andriessen 1990; Brown et al. 1993; Scheuber et al. 1995).

The igneous rocks in the Candelaria area (Fig. 1) represent Jurassic(?)–Early Cretaceous arc magmatism (Marschik and Fontboté 2001b). Volcanic and volcano–sedimentary deposits interfinger with an Early Cretaceous carbonate succession (Chañarcillo Group) that formed in a shallow marine back-arc environment to the east and southeast of Copiapó (e.g., Marschik and Fontboté 2001b). Marine deposition commenced in pre-Upper Valanginian times as shown by ammonites in the upper part of the volcanic–volcaniclastic Punta del Cobre Formation (Bandurrias Group; Marschik and Fontboté 2001b; Mourgues 2004; Fig. 2). From the late Valanginian to Aptian, carbonate rocks of the Chañarcillo Group accumulated to a thickness of 1,700–2,000 m (Corvalán 1974; Jurgan 1977a,b; Fig. 2). Basin inversion started in late Aptian times, resulting in regression and partial erosion of the back-arc sequence (e.g., Segerstrom and Parker 1959; Zentilli 1974; Jurgan 1977a,b; Arancibia 2004; Gana and Zentilli 2000; Mourgues 2004). Plutons of the Chilean Coastal Batholith intruded the Early Cretaceous arc/back-arc deposits in the west of the area. Their emplacement caused a wide contact metamorphic aureole near the town of Tierra Amarilla, south of Copiapó (latitude 27°30′S, Fig. 1; Tilling 1962, 1963a,b, 1976). In this area, the batholith intrusions have been grouped into the Copiapó plutonic complex (Marschik et al. 2003a).

Intrusive rocks

The Copiapó plutonic complex consists of several elongated or irregularly shaped, sub-alkaline to alkaline, magnetite-series volcanic arc I-type of plutons (Fig. 1). The plutonic rocks have initial $^{87}Sr/^{86}Sr$ from 0.7031 to 0.7032; initial $^{143}Nd/^{144}Nd$ from 0.51273 to 0.51278; and $^{206}Pb/^{204}Pb$, $^{207}Pb/^{204}Pb$, and $^{208}Pb/^{204}Pb$ from 18.43 to 18.77, 15.55 to 15.60, and 38.13 to 38.40, respectively, and $\delta^{18}O$ values from +6.9 to +8.6‰ (Marschik et al. 2003a). Calculated initial $^{187}Os/^{188}Os$ ratios for magmatic magnetite from plutons of the Copiapó complex are relatively homogeneous ranging from 0.21 to 0.41 (Mathur et al. 2002). These isotopic characteristics suggest the presence of mantle and crustal components in the batholithic rocks.

The Copiapó plutonic complex near the Candelaria mine (Fig. 1) comprises the following major units: pyroxene diorite (Kpd), hornblende diorite (Khd), monzodiorite (Kmd), quartz–monzonite porphyry (Kqm), tonalite (Kt), and granodiorite (Kgd, Fig. 1). The rocks of the pyroxene diorite unit are coarse-grained with hypidiomorphic granular to porphyritic textures. They are exposed west of the Candelaria tailings impoundments and west of the Alcaparrosa mine (Fig. 1). Bent plagioclase twin planes and undulatory extinction of most groundmass minerals in samples taken near the Alcaparrosa mine suggest that the

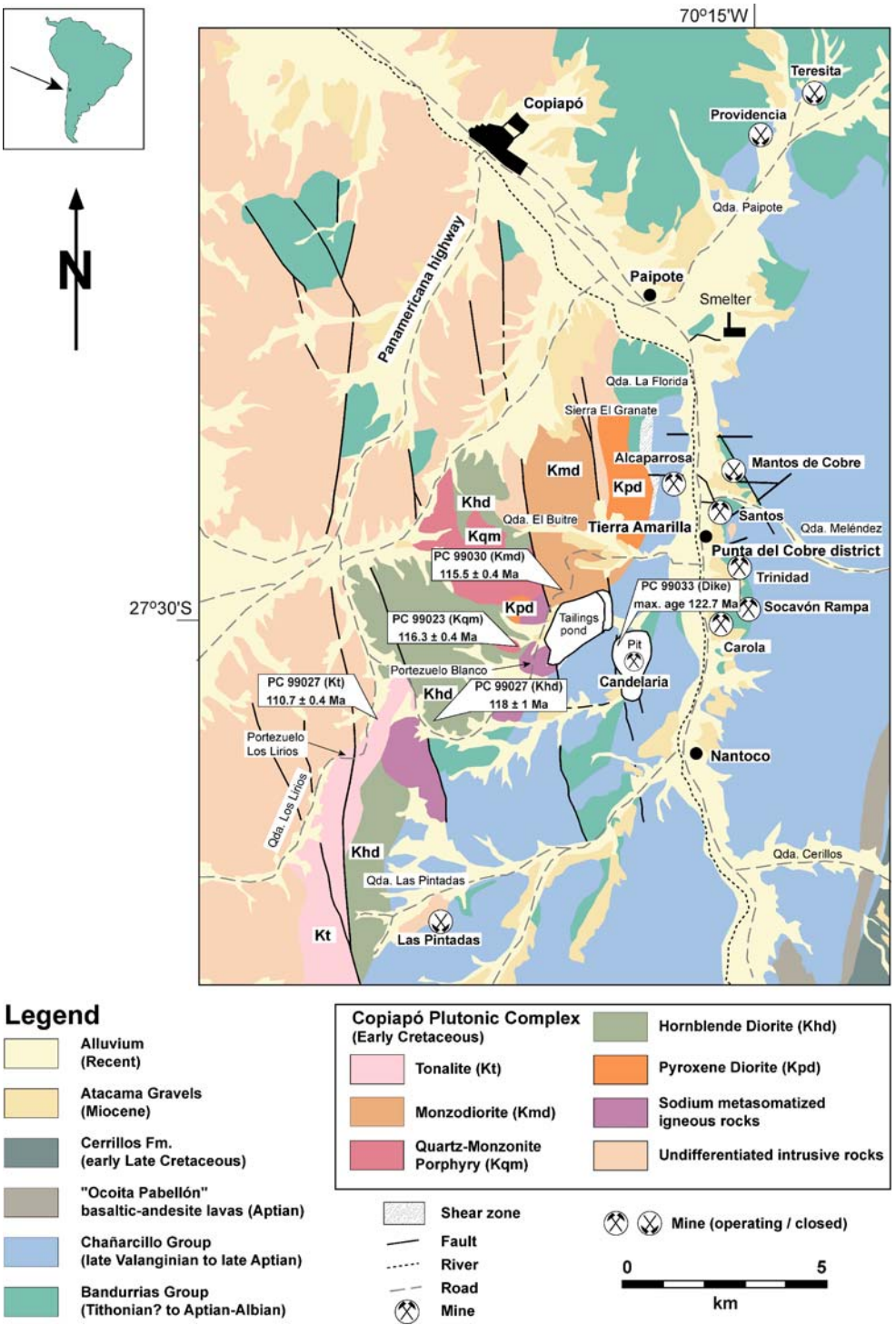

Fig. 1 Geologic map of the Candelaria–Punta del Cobre mining district showing the main units of the Copiapó plutonic complex (modified from Tilling 1976; Arévalo 1994, 1995). Sample locations and corresponding determined U–Pb zircon ages of the units are indicated

pluton is affected by shear deformation related to shear zones that occur locally along the eastern margin of the batholith (Marschik et al. 2003a).

The pyroxene diorite has gradational contacts with the hornblende diorite. The latter consists mainly of medium- to coarse-grained rocks with a hypidiomorphic granular texture. Hornblende diorite rocks exposed at Quebrada Las Pintadas (Fig. 1) have been dated at 111±3 Ma using the K–Ar method on biotite (Arévalo 1994; all geochronological data are reported at 2σ errors except when otherwise stated). The main outcrops of the quartz–monzonite porphyry unit are to the west of the Candelaria tailings impoundments (Fig. 1). The rocks of this unit contain plagioclase and occasionally amphibole phenocrysts in an

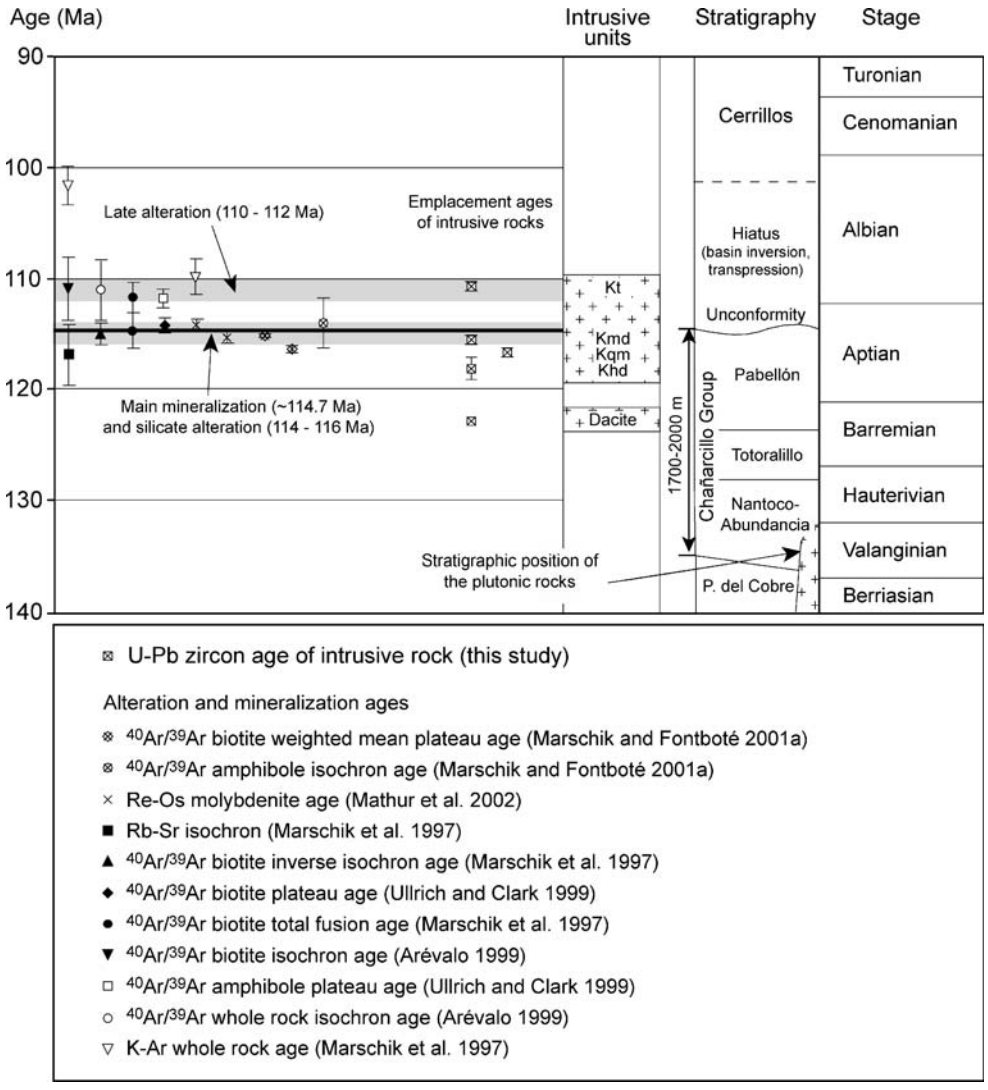

Fig. 2 Synthesis of relevant geochronological data on rocks and hydrothermal minerals from the Candelaria–Punta del Cobre district. Stratigraphic ages according to Gradstein et al. (1995)

orthoclase and quartz-rich matrix. They have SiO_2 and K_2O contents of around 65 and 5 wt%, respectively, and therefore show shoshonitic characteristics (Marschik et al. 2003a).

The quartz–monzonite porphyry has a north–northwest trending structural contact with the monzodiorite pluton, which is exposed to the north of the Candelaria tailings impoundments (Fig 1). Monzodiorite rocks are commonly medium- to coarse-grained, showing a hypidiomorphic granular texture. They have SiO_2 contents of around 60 wt% and show high-K characteristics with K_2O contents of around 3.2 to 4.6 wt% (Marschik et al. 2003a). Biotite from the monzodiorite unit yielded a $^{40}Ar/^{39}Ar$-weighted mean plateau age of 111.5±0.4 Ma (1σ; Arévalo 1999). The pyroxene diorite, hornblende diorite, and quartz–monzonite porphyry to the west and southwest of Candelaria are marginally affected by sodic or sodic–calcic alteration, whereas in the monzodiorite this type of alteration has not been recognized. Therefore, the monzodiorite is thought to be younger. A tonalite pluton occurs in the southwestern part of the study area at Quebrada Los Lirios (Fig. 1). The tonalite rocks represent a later intrusive event because they cut diorites and microgranitic dikes that are correlated with the quartz–monzonite porphyry unit (Tilling 1962). Several isotope ages are published on this unit including a K–Ar biotite age of 98.0±3.0 Ma (Zentilli 1974) and a K–Ar hornblende age of 69.0±4.0 Ma (Arévalo 1994). More recently, Arévalo (1999) reported a $^{40}Ar/^{39}Ar$ biotite-weighted mean plateau age of 109.8± 0.4 Ma (1σ) and a $^{40}Ar/^{39}Ar$ hornblende-weighted mean plateau age of 110.1±1.3 Ma (1σ). The outcrops of the granodiorite unit in the study area lie mainly at Sierra el Granate. There, the granodioritic rocks are medium-grained and show a hypidiomorphic granular texture.

The plutons intruded the lower part of the Chañarcillo Group around the time as these marine deposits reached

their maximum thickness in the late Aptian (Fig. 2). Therefore, the depth of pluton emplacement is probably around 1,700 to 2,000 m (Marschik et al. 2003a).

Lamprophyre, andesitic, dacitic, and aplite dikes are observed within the study area. Aplite and lamprophyre dikes cut batholithic and country rocks (e.g., Tilling 1962, 1976). An aplite hosting sulfide mineralization has been drilled at Candelaria (Marschik et al. 2003a). Lamprophyre dikes postdate mineralization in the Punta del Cobre district (Fig. 1), where they were emplaced mainly along the north–northwest to northwest-trending faults, which also control portions of the ore (Marschik and Fontboté 2001b). Dacite porphyry stocks, dikes, and sills are largely confined to the volcanic rocks and metasedimentary rocks adjacent to the batholith contact. These dacitic rocks show a close spatial relationship with mineralized zones within the district, though they are commonly barren or may be only weakly mineralized (e.g., locally in the Candelaria mine), respectively. Dacite porphyry stocks, dikes, and sills are affected by sodic, sodic–calcic, potassic or calc-silicate hydrothermal alteration (Marschik and Fontboté 1996, 2001a).

Relationship of iron oxide Cu–Au mineralization and magmatism

The major iron oxide Cu–Au ore bodies in the Candelaria–Punta del Cobre district are hosted in Early Cretaceous volcanic and volcaniclastic rocks near the eastern margin of the batholith (Fig. 1), within and just outside the contact metamorphic aureole. There are, however, several small mines and ore showings with a similar mineralogy within the batholithic rocks. La Candelaria is the largest mine in the area with 470 Mt at 0.95% Cu, 0.22 g/t Au, and 3.1 g/t Ag at a cutoff of 0.4% Cu and an output of over 200,000 t/year of Cu metal (Fig. 1; Marschik et al. 2000; Ministry of Mines, Chile 2002). The mineralization shows structural and litho-stratigraphic controls. The hypogene iron oxide-rich Cu–Au ore occurs mainly as veins, stringers, and as stratiform, breccia and replacement bodies. Pre-ore ductile deformation was accommodated by north–northeast trending shear zones that occur at or close to the batholith contact and at Candelaria. Some of the early magnetite at Candelaria is affected by shear deformation. Most of the copper vein and breccia ores are controlled by northwest to north–northwest trending faults. Reactivation and post-mineralization block faulting with a sinistral strike–slip component occurred along these northwest to north–northwest trending faults displacing the Candelaria orebody.

Results of previous stable and radiogenic isotope studies are coherent with a significant magmatic fluid, metal, and sulfur component in the ore-forming hydrothermal system. Sulfides have $\delta^{34}S_{CDT}$ values mainly between −3.2 to +3.1‰ (Rabbia et al. 1996; Marschik et al. 1997; Ullrich and Clark 1999; Marschik and Fontboté 2001a), though some values of up to +7.2‰ have been reported (Rabbia et al. 1996; Ullrich and Clark 1999) suggesting the presence of sulfur from magmatic and locally also non-magmatic sources. The calculated isotopic composition of a fluid in equilibrium with ore-related quartz lies between +5.9 and +8.9‰ $\delta^{18}O_{SMOW}$ for a temperature range from 370 to 440°C (using isotope fractionation factors of Friedman and O'Neil 1977) that is based on microthermometric measurements on fluid inclusions in the ore-related quartz (Marschik et al. 2000). These results point towards a magmatic–hydrothermal fluid contribution or participation of non-magmatic fluids equilibrated with silicates at high temperatures. The isotopes of chlorine, strontium, and Cl/Br ratios in fluid inclusions in ore-stage quartz from Candelaria suggest mixing between fluids from mantle-derived magmatic Cl and crustal brine Cl reservoirs (Chiaradia et al. 2006). Lead of ore minerals has the same isotope composition as the unaltered batholitic and volcanic rocks of the area (Marschik et al. 2003b), suggesting derivation of the ore lead, and by inference also Cu, directly from a hydrothermal fluid exsolved during crystallization of the batholithic magmas and/or from hydrothermal leaching of the altered volcanic rocks. Finally, the similarity in initial $^{187}Os/^{188}Os$ of the ore of 0.36±0.1 and magmatic magnetite in the plutons ranging from 0.21 to 0.41 supports the hypothesis that the plutonic magmas are the source for metals in the Candelaria–Punta del Cobre district (Mathur et al. 2002). However, none of these studies could link so far the mineralizing fluid to a particular intrusive phase in the area.

The age for the metallic mineralization at Candelaria is represented by molybdenite Re–Os ages of 114.2±0.6 Ma and 115.2±0.6 Ma (Mathur et al. 2002). The ages of the silicate alteration minerals associated with iron oxide Cu–Au ore in the Candelaria–Punta del Cobre district can be broken into an older group of about 114 to 116 Ma and a younger group of 110 to 112 Ma. A compilation of the relevant geochronological data is given in Fig. 2 (see also Marschik and Fontboté 2001a for details).

Sampling and analytical techniques

Representative samples were collected from four units of the Copiapó plutonic complex and from a dacite porphyry dike–sill complex exposed in the open pit of the La Candelaria mine (Fig. 1). A monzodiorite sample (PC 99030) was collected from a road cut along the road Tierra

Amarilla–Candelaria, at kilometer 9.790 from the town of Tierra Amarilla. The sample comes from an outcrop that also exposes tourmaline-bearing aplitic dikes, which cut the monzodiorite. The quartz–monzonite porphyry unit (PC 99023) was sampled from an outcrop to the northwest of Portezuelo Blanco, about 150 m west of the road between Tierra Amarilla and the Candelaria mine. A sample from the hornblende diorite unit (PC 99027) was taken to the north of the road between the Candelaria mine to the east and the Panamericana highway in the west. The tonalite unit (PC 99025) was sampled in a valley to the north of Portezuelo Los Lirios, and a sample of the dacite porphyry dike–sill complex (PC 99033) comes from the pushback of the Candelaria open pit.

U–Pb zircon isotope analysis was carried out at the Department of Earth and Environmental Sciences, Ludwig-Maximilians Universität, Munich, Germany. Heavy mineral separates were obtained using jaw crusher, roller mill, shaking table, and magnetic separator at the Department of Geosciences, University of Arizona, Tucson, USA. All obtained zircon separates were further purified by hand-picking using only optically pure grains for analysis. Before spiking, all mineral separates were cleaned in an ultrasonic bath with quartz-distilled 6 N HCl, twice deionized, quartz-distilled water, and Medison-distilled acetone.

Zircon fractions were treated using the standard methods described by Krogh (1973, 1982). Samples were split after dissolution leaving two-thirds of the solution unspiked and adding a $^{208}Pb/^{235}U$ mixed spike to the remaining one third. Isotopic ratios of Pb and U were determined using a Finnigan MAT 261/262 multi-collector mass spectrometer in static mode. Pb blanks did not exceed 20 pg. The following values were used for the composition of the Pb blank: $^{206}Pb/^{204}Pb=18.15$, $^{207}Pb/^{204}Pb=15.63$, $^{208}Pb/^{204}Pb=38.14$. Common Pb corrections were done using either Pb isotopic ratios from whole rock residues (Marschik et al. 2003a) adapted to the age of intrusion or the model of Stacey and Kramers (1975). For 3-D planar or linear regression calculations, we used equations from ISOPLOT 2.49 program (Ludwig 2001). U–Pb data were evaluated using the programs PBDAT and ISOPLOT/EX 2.49 of Ludwig (1993, 2001), respectively. Error ellipses shown in the figures below, as well as given age errors, are at the 2σ level. Thorium concentrations were calculated from ^{208}Pb concentrations. Decay constants used are those recommended by the IUGS (Steiger and Jäger 1977).

Zircon characteristics and analytical results

The results of U–Pb zircon geochronology are summarized in Tables 1 and 2. The units are discussed in chronological order regarding zircon crystallization ages. The zircons of

Table 1 Sample location and U–Pb zircons ages

Sample	Rock type	Latitude	Longitude	Intrusion age $\pm 2\sigma$ (Ma)	Pb (common) isotope composition		Comments	
					$^{206}Pb/^{204}Pb_{com}$	$^{207}Pb/^{204}Pb_{com}$	Method of Pb correction	
PC 99033	Dacite porphyry dike	27°30′43″S	70°17′52″W	122.7±0.5[a]	24.840	15.900	Stacey and Kramers (1975) model	Concordia age of 1 point, μ=9.74 (2 discordant points)
PC 99027	Hornblende diorite (Khd)	27°32′00″S	70°20′52″W	118±1	18.442	15.591	WR-residue, Marschik et al. (2003a)	Concordia age of 3 points, μ=9.63, Pb-model age 1,635 Ma
PC 99023	Quartz–monzonite porphyry (Kqm)	27°30′24″S	70°19′24″W	116.3±0.4	18.593	15.644	WR-residue, Marschik et al. (2003a)	Concordia age of 2 points, μ=9.83, Pb model age, 160 Ma
PC 99030	Monzodiorite (Kmd)	27°29′46″S	70°18′14″W	115.5±0.4	18.349	15.557	WR-residue Marschik et al. (2003a)	Discordia of 4 points (2 concordant points) μ =9.51, Pb-model age=1350 Ma
PC 99025	Tonalite (Kt)	27°32′15″S	70°22′24″W	110.7±0.4	18.405	15.557	WR-residue, Marschik et al. (2003a)	Discordia of 4 points, concordant points, μ=9.57, Pb model age ~2,414 Ma

[a] Analytical error on the measurement of one grain-size fraction

Table 2 Zircon characteristics and analytical results

Sample	Zircon characteristics			Contents				Meas.		Calculated atomic ratios					Apparent ages (Ma)		
	Appearance[a]	Type	Grain size (μm)	U (ppm)	Th[b] (ppm)	Th/U	Pb_{tot} (ppm)	$^{206}Pb/^{204}Pb$	$^{206}Pb/^{238}U$	2σ%	$^{207}Pb/^{235}U$	2σ%	$^{207}Pb/^{206}Pb$	2σ%	$^{206}Pb/^{238}U$	$^{207}Pb/^{235}U$	$^{207}Pb/^{206}Pb$
Dacite dike (PC 99033)																	
1	A2, shp, subhedral	S13	50–80	129.8	104	0.80	2.981	582	0.018995	0.630	0.15798	6.70	0.060321	6.22	121.3	148.9	615.1
2	A2, p, total fraction	S13	<65	140.3	161.3	1.15	4.399	191	0.020242	1.238	0.28366	9.80	0.101635	8.62	129.2	253.6	1654
3	A2, p, euhedral transparent	S13	80–125	183.4	147.9	0.81	4.856	230	0.019210	0.368	0.12850	1.90	0.048515	1.762	122.7	122.8	124.5
	$Pb_{(com)}$ correction according to the model of Stacey & Kramers (1975) for 122 Ma																
Hornblende diorite (PC 99027)																	
1	A2, shp, pink, transparent	P5, D, S24-S12	90–130	337.8	225	0.67	7.91	314	0.018365	0.456	0.12184	1.326	0.048117	1.180	117.3	116.7	105
2	A2, shp, pink, transparent	P5, D, S24-S12	50–80	300.1	166	0.55	6.36	747	0.018671	1.142	0.12444	1.612	0.048339	1.076	119.3	119.1	115.9
3	A2, pink fragments	P5, D, S24-S12	60–120	269.1	261	0.97	6.72	274	0.018128	0.670	0.12331	1.160	0.049460	0.898	115.8	118.3	169.7
4	A2, total	P5, D, S24-S12	<50	276.7	146	0.53	5.7	866	0.018451	0.470	0.12363	1.006	0.048471	0.822	117.9	118.1	122.3
	$Pb_{(com)}$ correction: $^{206}Pb/^{204}Pb$=18.442; $^{207}Pb/^{204}Pb$=15.5912 according to WR-residue for 118 Ma																
Quartz–monzonite porphyry (PC 99023)																	
1	A1/A2, elp+p, colorless, anhedral	P (P5?)	100–200	907.4	3113	3.43	24.85	178	0.018224	0.406	0.12204	0.878	0.048567	0.744	116.4	116.9	127.0
2	A1/A2, elp+p, colorless, anhedral	P	61–100	1144.2	1099	0.96	25.33	663	0.018167	0.692	0.12153	1.096	0.048519	0.804	116.1	116.5	124.7
	$Pb_{(com)}$ correction: $^{206}Pb/^{204}Pb$=18.593; $^{207}Pb/^{204}Pb$=15.644 according to WR-residue at 116 Ma																
Monzodiorite (PC 99030)																	
1	A2, p, colorless, transparent	P5	200–300	872.9	815	0.93	18.85	1377	0.018165	0.358	0.12302	0.720	0.049117	0.592	116.0	117.8	153.4
2	A2, pink, many fragments	P5	100–150	677.0	541	0.80	14.22	1003	0.018141	0.350	0.12157	0.419	0.048600	0.222	115.9	116.5	128.6
3	A2, pink, only fragments	–	80–100	749.8	846	1.13	17.23	618	0.018119	0.366	0.12136	0.646	0.048577	0.506	115.8	116.3	127.5
4	A2, p, colorless, transparent	P5	<80	649.5	1062	1.64	16.65	540	0.018073	0.356	0.12087	0.540	0.048505	0.390	115.5	115.9	124.0
	$Pb_{(com)}$ correction: $^{206}Pb/^{204}Pb$=18.3496; $^{207}Pb/^{204}Pb$=15.557 according to WR-residue at 116 Ma																
Tonalite (PC 99025)																	
1	A2, p, euhedral, transparent	S	60–100	198.2	145	0.73	3.89	652	0.017047	3.66	0.11465	3.88	0.048778	1.22	109.0	110.2	137.2
2	A2, p, euhedral, translucent	S	100–150	205.2	118	0.57	3.94	790	0.017346	0.34	0.11697	0.70	0.048905	0.60	110.9	112.3	143.3
3	A2, p+elp, euhedral, translucent	S+S4	150–180	144	219	1.52	3.92	159	0.017738	0.36	0.14460	12.56	0.059123	12.56	113.4	137.1	571.6
4	A2, elp, euhedral, transparent	S4	100–125	174.46	130	0.75	3.62	535	0.017668	0.38	0.13986	2.20	0.057412	2.02	112.9	132.9	507.4
	$Pb_{(com)}$ correction: $^{206}Pb/^{204}Pb$=18.405; $^{207}Pb/^{204}Pb$=15.575 according to WR-residue at 111 Ma																

$Pb_{(blank)}$ correction: $^{206}Pb/^{204}Pb$=18.15, $^{207}Pb/^{204}Pb$=15.63, $^{208}Pb/^{204}Pb$=38.14 (for 0.02 ng Pb-blank)

[a] Shape, type: *A* euhedral to subhedral, type according to Pupin (1980); surface structure: *1* often dark-colored, dim, pitted surface, metamict; *2* often pale-colored, transparent to translucent; *p* prismatic; *shp* short prismatic; *elp* elongated prismatic

[b] Th calculated from $^{208}Pb/^{206}Pb$ ratio; Pb mass discrimination = 0.13% per amu

the investigated igneous rocks have been classified using the typology model of Pupin (1980, 1985). Cathode luminescence images of selected grains are shown in Fig. 3.

Dacite porphyry dike–sill complex

Zircon characteristics

Zircons of the dacite porphyry dike (sample PC 99033) are euhedral to sub-rounded, colorless to pale pink colored, and transparent to translucent with pitted crystal faces. Rounding of edges and pyramidal apices are due to magmatic corrosion. The decrease in transparency of the zircons coincides with the increase in color intensity and surface corrosion phenomena. Euhedral zircons are prevalently free of inclusions and commonly characterized by dull pyramidal apices, which seem to have grown onto earlier corroded (sub-rounded) pyramidal apices. Despite modification of the zircon shapes due to magmatic corrosion, the zircon type can be identified. The zircons in the dacite porphyry dike represent a single population (Pupin 1980) that can be denoted as S13-type, with equally developed prisms (100) and (110) and pyramidal faces (101) and (211). According to Pupin (1980), this zircon type is commonly derived from calc-alkaline series granodiorites and monzogranites of hybrid crustal and mantle origin.

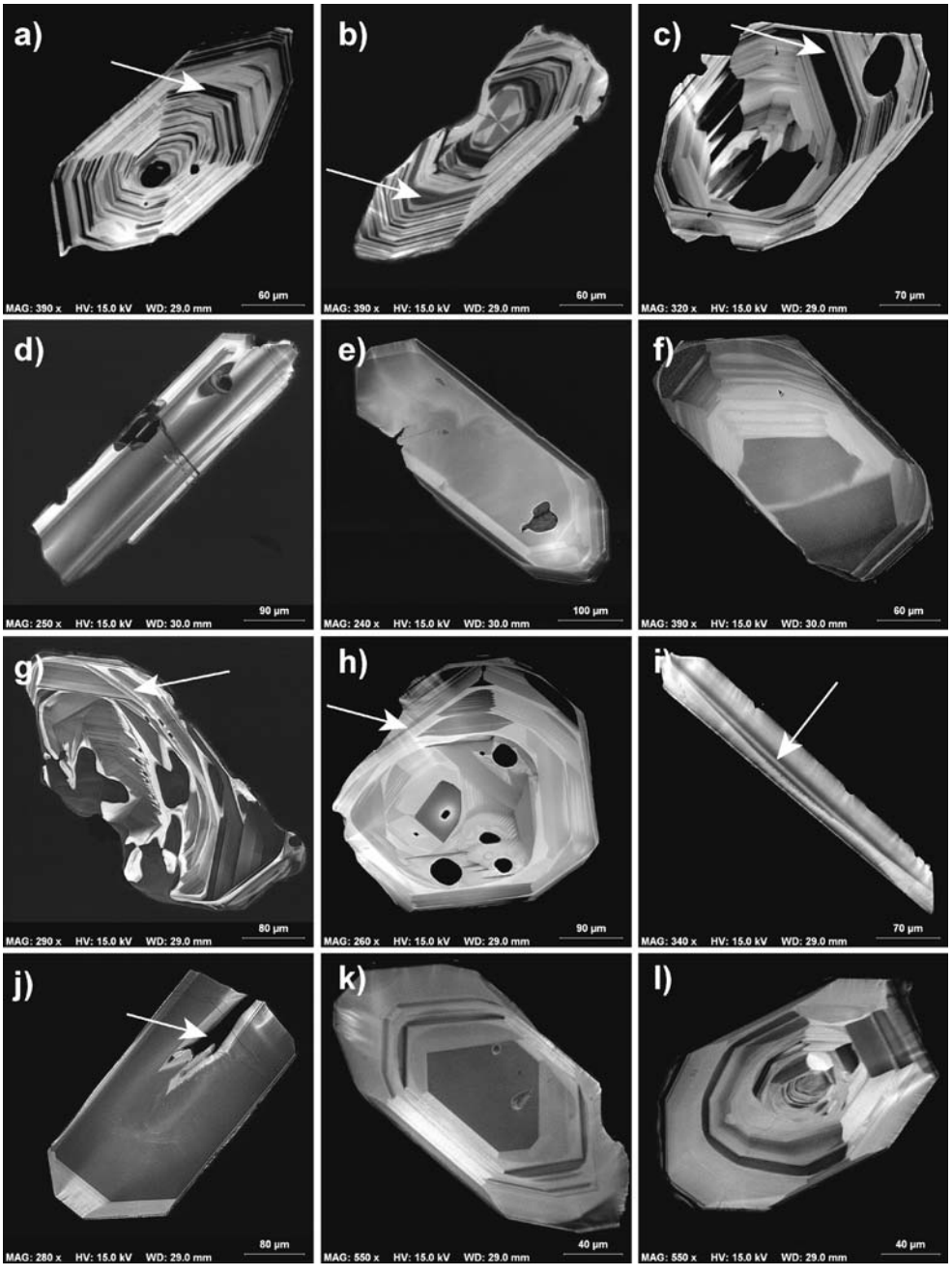

Fig. 3 Cathode luminescence images of zircons from the dated igneous rocks. **a**–**c** Zircons of the dacite porphyry dike–sill complex (PC 99033) contain nuclei, which have coherent boundaries with the outer zones. The zircons are characterized by oscillatory and sector zoning. Dissolution surfaces truncating growth zones are observed. In many of the zircon, there is a well-developed, more or less wide zone of low luminescence (dark zone; see *arrows*). **d**–**f** Zircons of the hornblende diorite (PC 99027) display a homogenous inner domain with lower and an outer domain commonly with higher luminescence. The crystals lack any visible seed crystal or an inherited core. **d**,**e** The predominantly developed steep pyramid (211) suggests zircon S type characteristics. **g**,**h** Zircons of the quartz–monzonite porphyry (PC 99023) lack inherited cores. Sector zoning is well-developed. A dissolution surface separates a voluminous, heterogeneous inner domain from an outer domain (see *arrows*). Mineral inclusions without or very low luminescence are common. **i** Elongated prismatic zircon from the monzodiorite (PC 99030) hosting a medial tube with low luminescence surrounded by a dark reaction rim (see *arrow*). **j**–**l** The zircons of the tonalite (PC 99025) are characterized by a homogeneous outermost growth zone; they may or may not contain a medial tube filled opaque material (**j**, see *arrow*) or a dark central zone (**k**) or an inherited core (**l**)

Three grain-size fractions were prepared for U–Pb analysis. Fraction 1 consists mostly of short prismatic crystals with sizes between 50 and 80 μm. Fraction 2 is composed of complete crystals and crystal fragments with sizes <65 μm, and fraction 3 contains euhedral prismatic crystals with sizes of 80 to 125 μm. Only fraction 3 is enriched in transparent, colorless crystals and incorporation of fragments has been avoided.

Cathode luminescence images are shown in Fig. 3a–c. They reveal that the zircons contain nuclei, which have coherent boundaries with the outer zones. Dissolution surfaces are observed truncating growth zones. The crystals are characterized by oscillatory and sector zoning. Zones of high or low luminescence reflect low or high trace element concentrations, respectively (Sommerauer 1976). In most of the zircon, there is a well-developed, more or less wide, zone of low luminescence (dark zone; Fig. 3a–c).

Analytical results

Uranium and thorium contents in all grain-size fractions are low (U=130 to 183 ppm; Th=104 to 148 ppm) and show a positive correlation between increasing U contents and increasing grain size. Common lead concentrations in the zircons are high ($^{206}Pb/^{204}Pb$ ratios from 202 to 774). In the absence of whole rock Pb isotopic data on this sample, we use the $Pb_{(com)}$ correction model of Stacey and Kramers (1975) with μ=9.74. The data of fraction 3 plot on the Concordia at 122.7 Ma, whereas the data points 1 and 2 are discordant (Fig. 4). Therefore, the analytical error of ±0.5 Ma on the age, defined by fraction 3, cannot be taken as measure of accuracy of this age. The discordant data suggest that the Pb isotope system in parts of the zircons is disturbed. A 3-D planar regression model, after Ludwig (2001), applied to the data of all three fractions also points to a disturbed Pb isotope system. Calculations result in anomalous common Pb ratios ($^{207}Pb/^{204}Pb$=15.9 and $^{206}Pb/^{204}Pb$=24.839). If anomalous ^{206}Pb enrichment is assumed, data points in a 3-D planar regression model would fit a regression line providing a younger intercept age of around 119 Ma. Positions of data points 1 and 2 in the Concordia diagram of Fig. 4 suggest the presence of an inherited radiogenic lead component and a loss of radiogenic lead and/or gain of uranium compared to the concordant data point 3. We assume that the dominant dark zone mentioned above may have incorporated externally derived uranium and radiogenic lead, which is responsible for discordance of the data points 1 and 2. We consider the age of about 123 Ma of fraction 3 as a maximum age for the emplacement of the dacite porphyry dike–sill complex.

Hornblende diorite unit (Khd)

Zircon characteristics

Zircons of the hornblende diorite (sample PC 99027) are pink and transparent. The larger zircon crystals (>150 μm)

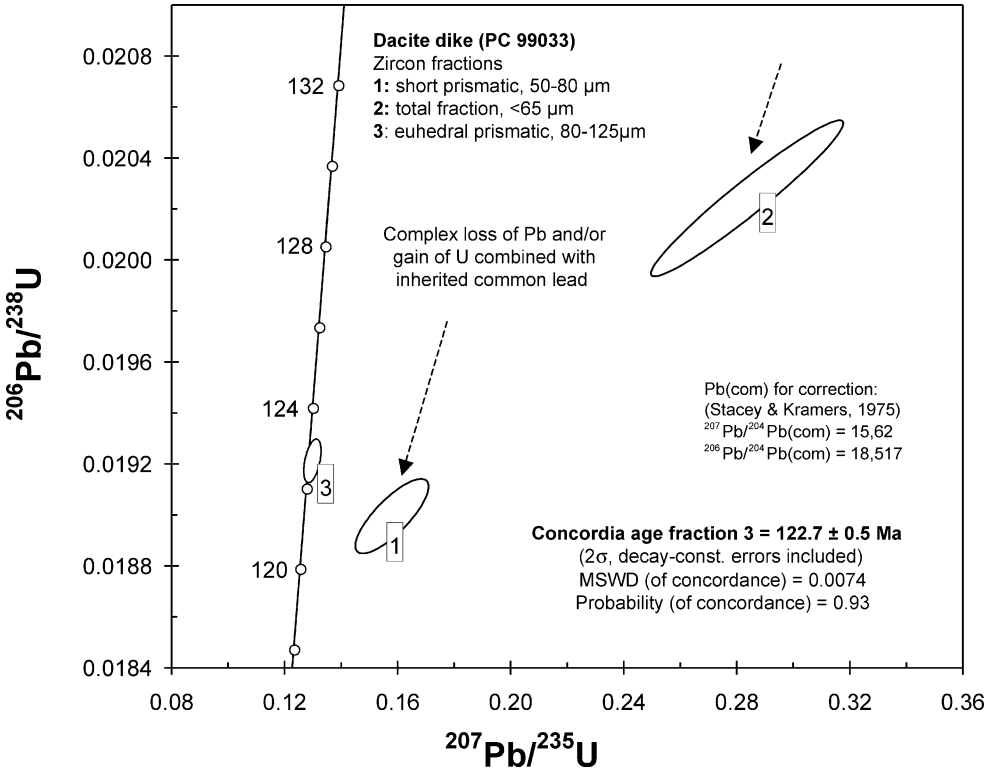

Fig. 4 U–Pb Concordia diagram of sample PC 99033 from the dacite porphyry dike–sill complex in the Candelaria mine. Data points of grain-size fractions are concordant (fraction 3) and discordant (fractions 1 and 2). Discordant position of fraction 1 with an $^{206}Pb/^{238}U$ age less than that of the concordant fraction 3 seems to indicate that discordance of all fractions may derive from composite loss of radiogenic Pb and/or U gain combined with inherited common lead. An age calculation from these fractions is therefore irrelevant. The Concordia age of fraction 3 at 122.7 Ma is interpreted as the time of zircon crystallization and represents a maximum value for the age of intrusion of the dacite porphyry dike–sill system. The analytical error of ±0.5 Ma on the age defined by fraction 3 cannot be taken as measure of accuracy of this age

are commonly broken into fragments along marked fracture lines perpendicular to the long axis. The zircons commonly show a central channel filled with opaque mineral phase(s). Zircons of the hornblende diorite can be classified into P5-, D-, and S-types (Pupin 1980, 1985). Zircons assigned to the P5- and D-type categories are predominant. The zircons with S-type characteristics are nearly identical in transparency and color to the P-type zircons. S-type zircons either appear as homogeneous single crystals or are directly grown on corroded remnants of P-type zircons. The most striking aspect is the complete lack of inclusions in the S-type zircon generation. They show continuous variations in shape from S24- to S12-types. The presence of P5-, D-, and S-types suggests zircon crystallization during more than one stage of magma development. According to Pupin (1980, 1985), P5- and D-type zircons crystallize in alkali series granites of mainly mantle origin, whereas S-type zircons commonly are formed from crustal magma sources. The occurrence of S24- to S12-types can be interpreted as a gradual change in magma composition by crustal assimilation processes, reaching a tonalitic end member (distribution area "T." for tonalite; Pupin 1980).

Cathode luminescence images of selected crystals are given in Fig. 3d,e. They show a homogenous darker inner domain, a lighter outer overgrowth, and do not contain any visible seed crystal or an inherited core.

The fragmentation during zircon processing was intense due to the presence of numerous cracks in the zircon crystals. Zircons were separated into grain-size fractions but could not be further differentiated based on crystal shapes. Fractions 1 and 2 consist of euhedral, short prismatic crystals of 90 to 130 μm or 50 to 80 μm, respectively. Fraction 3 is composed of zircon prism fragments without pyramidal apices (60 to 120 μm). Fraction 4 consists of small zircons (<50 μm) and includes crystals and crystal fragments.

Analytical results

The zircons of the hornblende diorite have uranium contents from 269 to 338 ppm and thorium contents from 166 to 261 ppm. High quantities of common Pb in zircons ($^{206}Pb/^{204}Pb$ from 274 to 866) require Pb_{com} corrections. Pb isotope ratios of "leachates" and "residues" are known from leaching experiments on equivalent whole rock (WR) samples (Marschik et al. 2003a). Both $^{206}Pb/^{204}Pb$ ratios of "WR leachates" and "WR residues" are slightly depleted in radiogenic lead compared with calculated values from the Stacey and Kramers (1975) model (μ=9.74). The Pb model age of 1,635 Ma is based on the mean value of Pb isotope ratios from residues of the hornblende diorite (samples PC 97006, PC 97007, PC 97008 in Marschik et al. 2003a), which are recalculated to a crystallization age of 118 Ma and adapted to the Pb evolution model of Stacey and Kramers (1975), and a μ-value of 9.63 corresponding to $^{206}Pb/^{204}Pb$=18.442 and a $^{207}Pb/^{204}Pb$=15.591.

Figure 5 shows the results in a Concordia diagram. The data points of fractions 1, 2, and 4 are concordant at 117.7±0.4 Ma (2σ; probability of concordance=0.82; MSWD of concordance=0.049; Concordia age after Ludwig 2001). Fraction 3 data are slightly discordant in the Concordia diagram (Fig. 5) because of an inherited radiogenic lead component and have been omitted from the age calculation. Fraction 2 has somewhat higher Pb/U ages than fractions 1 and 4, which may also result from an inherited radiogenic lead component. Therefore, an age of 118±1 Ma seems more realistic. This age represents the maximum age of the zircon crystallization and of hornblende diorite emplacement.

Quartz–monzonite porphyry unit (Kqm)

Zircon characteristics

Zircons of the quartz–monzonite porphyry (sample PC 99023) are colorless and transparent. The shapes are predominantly subhedral to rarely anhedral. Whitish dull pyramidal apices, rounded edges, and pitted crystal faces are caused by magmatic corrosion. The degree of magmatic dissolution makes it difficult to determine the characteristics for the zircon type (Pupin 1980). The original P5-type characteristics can be inferred from rarely preserved, euhedral, elongated, prismatic zircons.

Cathode luminescence images show zircons without inherited cores (Fig. 3g,h). A voluminous, heterogeneous inner domain is separated by a dissolution surface from an outer domain with well-developed sector zoning. A pronounced dark boundary zone between the two domains, as observed, e.g., in zircons from the dacite porphyry dike, is not developed. Mineral inclusions with no or very low luminescence are common.

The large proportion of dull, brownish zircons argues for metamictization, due to high U and Th contents (see below). These metamict crystals were omitted from analysis. Two grain-size fractions (fraction 1, 100 to 200 μm; fraction 2, 61 to 100 μm) were prepared for analysis.

Analytical results

Data points of grain-size fractions 1 and 2 are concordant at 116.3±0.4 Ma (2σ; probability of concordance=0.13; MSWD of concordance=2.2; Concordia age calculated according to Ludwig 2001; Fig. 6). The probability for X–Y equivalence and Concordance is 0.54; therefore, the error of the Concordia age is appropriate (Ludwig 2001).

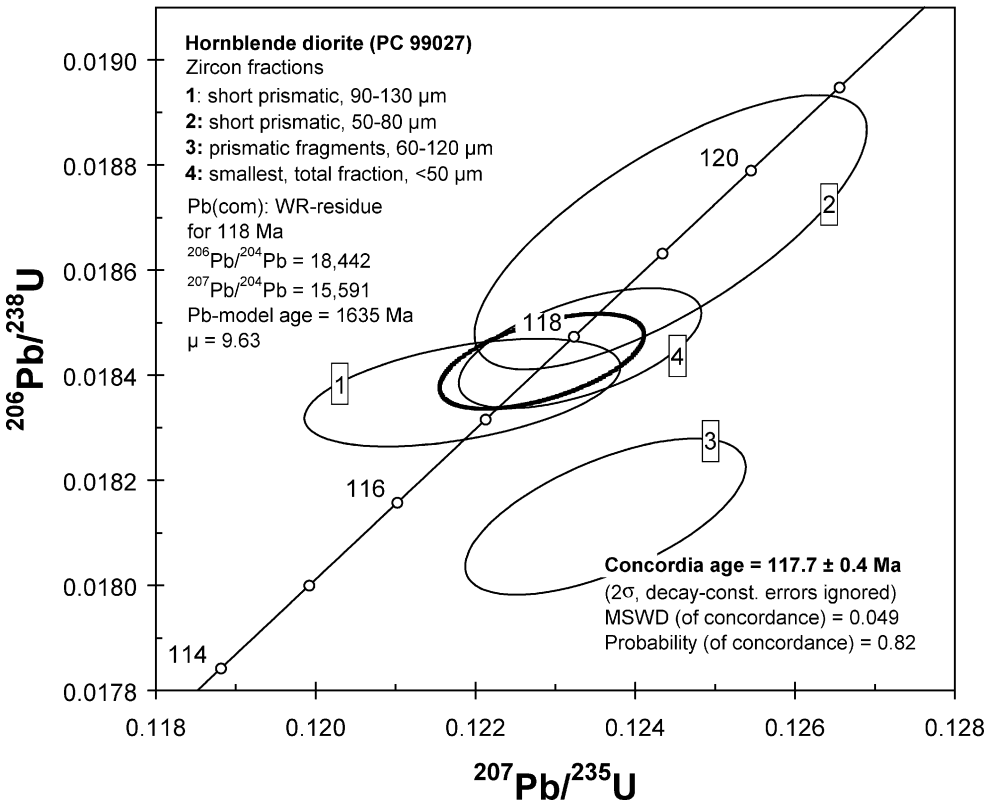

Fig. 5 U–Pb Concordia diagram of sample PC 99027 from the hornblende diorite (Khd) unit. Three data points representing grain-size fractions 1, 2, and 4 are concordant at 117.7± 0.4 Ma (Concordia age, Ludwig 2001). Fraction 3 data are slightly discordant in the Concordia diagram and have been omitted from the age calculation. Fraction 2 has somewhat higher Pb/U ages than fractions 1 and 4, which may result from an inherited radiogenic lead component. Therefore, an age of 118±1 Ma seems more realistic. This age is interpreted as the time of zircon crystallization and thus, represents the maximum age for the emplacement of the hornblende diorite

This age is interpreted as zircon crystallization age, which represents the maximum age for the intrusion of the quartz–monzonite porphyry. High common Pb quantities in zircons ($^{206}Pb/^{204}Pb$ ratios are 178 and 663) require individual common Pb correction. We used Pb isotope ratios of residue of the whole rock sample PC 97004 from the

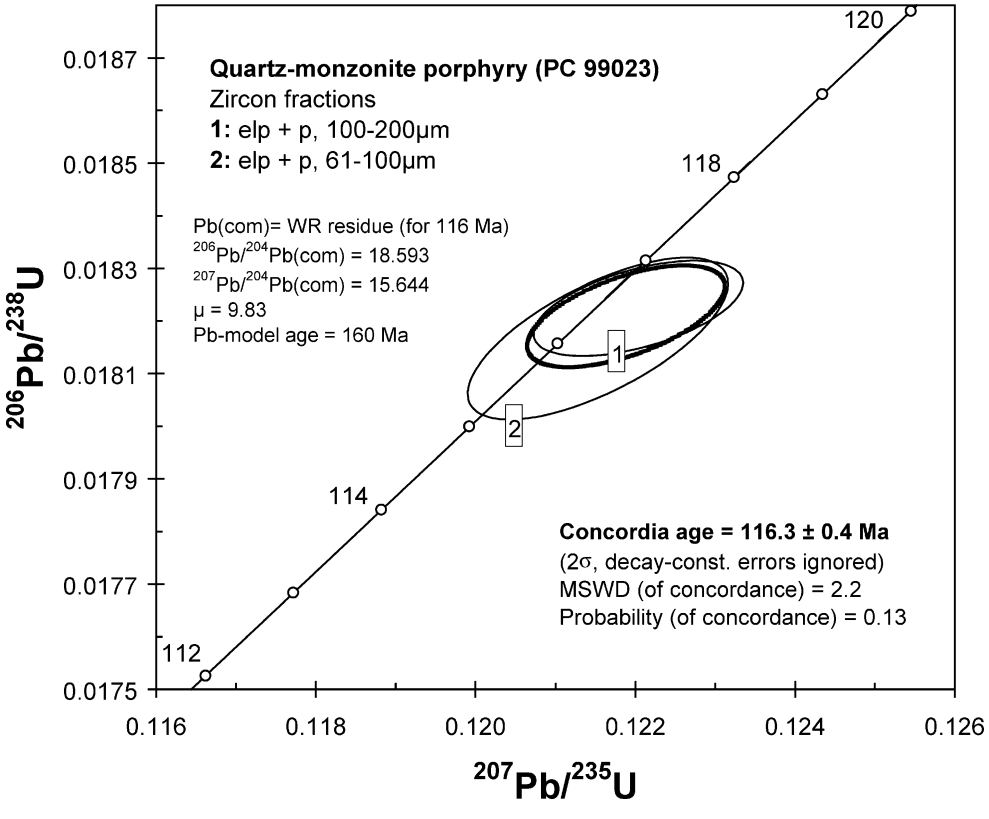

Fig. 6 U–Pb Concordia diagram of sample PC 99023 from the quartz–monzonite porphyry (Kqm) unit. Data points of grain-size fractions are concordant at 116.3±0.4 Ma (Concordia age, Ludwig 2001). The age represents the time of zircon crystallization and represents the maximum emplacement age

quartz–monzonite porphyry unit given in Marschik et al. (2003a). These Pb ratios recalculated for the time of formation at 116 Ma ($^{206}Pb/^{204}Pb$=18.593; $^{207}Pb/^{204}Pb$=15.644) provide a μ-value of 9.83 and a Pb model age of 160 Ma. This may suggest assimilation and homogenization of crustal Pb in the mantle-derived melt. Uranium and thorium concentrations in zircons are high (U=907 and 1,144 ppm; Th=1099 and 3,113 ppm) and exceed the elevated concentrations in the monzodiorite (Table 2; see sample PC 99030 below). These high U and Th concentrations are consistent with the shoshonitic character of these rocks (Marschik et al. 2003a).

Monzodiorite unit (Kmd)

Zircon characteristics

The zircon populations of the monzodiorite (sample PC 99030) are heterogeneous. The rock contains large zircon crystals (up to 500 μm long) but also many crystal fragments. Zircons can be distinguished according to transparency and color. Euhedral, transparent, and colorless to pale pink zircons commonly contain a medial tube in their central domain, which is filled with opaque (hematite?) or transparent materials (probably liquid/melt inclusions). The zircon type can be characterized as P5 [Pupin 1980; prisms (100)>>(110) and pyramidal apex (101)]. They commonly show an irregularly formed, edge-rounded, anhedral overgrowth, which possibly formed during a second crystallization phase under different melt conditions.

Cathode luminescence investigations suggest homogenously developed zircons. Inherited cores are lacking. High or low luminescent rims envelop the medial tubes (Fig 3i), mentioned above. These rims are presumably caused by the chemical reaction between the host zircon and tube filling.

Uranium (650 to 873 ppm) and thorium (541 to 1062 ppm) contents are high. There are also zircons, which are similar in type (P3/P5) but are brown, totally dull, and with scarred surfaces, suggesting that they experienced strong metamictization. These zircons were omitted from analysis.

Four grain-size fractions were prepared for analysis. Grain-size fraction 1 (200 to 300 μm) and 4 (<80 μm) consist predominantly of euhedral and colorless P5-type zircons. The fractions 2 (100 to 150 μm) and 3 (80 to 100 μm), in contrast, are composed almost completely of crystal fragments.

The zircon types can be used to estimate temperatures and alkalinities of melts (Pupin 1980, 1985). P5-type zircons, which are the most abundant in the monzodiorite, are suggestive of melts of alkaline series granites of mainly mantle origin and melt temperatures in excess of 800°C. This is consistent with geochemical and isotope geochemical characteristics (Sr initial ratio ~0.70315 and εNd ~5.6) of these rocks (Marschik et al. 2003a).

Analytical results

The uranium and thorium concentrations in zircons of the monzodiorite are between 650 and 873 ppm or between 541 and 1062 ppm, respectively. Discordia calculation (Ludwig 2001) based on all grain-size fractions yields a lower intercept age of 115.5±0.4 Ma (2σ; probability of fit=0.43; MSWD=0.83; according to Ludwig 2001; Fig. 7). This age is interpreted as the time of zircon crystallization and gives a maximum age for the magma emplacement. The discordance of fractions 1 and 2 cannot be attributed to inherited older lead components because of the lack of inherited cores. Reasons for this discordance may lie in the zircon crystallization itself. Presence of median tubes, filled with opaque material or transparent liquids/fluids, are certainly a trap for inherited lead (Fig. 3i).

Common Pb correction in zircons was done using Pb isotopic ratios of the equivalent whole rock residue analysis of the monzodiorite (samples PC97002/03) given in Marschik et al. (2003a). The corresponding μ-value is 9.51. Calculations based on the Stacey & Kramers' two-stage model for lead isotopic evolution (Stacey and Kramers 1975) using Pb isotopic ratios ($^{206}Pb/^{204}Pb$=18.349; $^{207}Pb/^{204}Pb$=15.557), similar to those of the whole rock residues but adapted to crystallization age of 116 Ma, and a μ-value of 9.51, yields a model age of 1,350 Ma. This Pb model age is inconsistent with this upper Concordia intercept age of about 2,840 Ma. We assume that the Pb isotope system in zircon of large grain size is disturbed, because of the presence of median tubes, which are more abundant in these zircons. The μ-value is below that of "average active terrestrial lead" (9.74; Stacey and Kramers 1975), but tends to that of the mantle (8.35; Zartman and Doe 1981), supporting the hypothesis of a mantle component in the melt. This is consistent with the zircon types and geochemical data mentioned above (Marschik et al. 2003a).

Tonalite unit (Kt)

Zircon characteristics

Zircons from the tonalite (PC 99025) form a homogeneous population with respect to properties observed under the microscope. They are euhedral, transparent to translucent, and colorless. Shapes are mainly short prismatic (length/width=1.5 to 2, rarely 3). Tube- and drop-shaped inclusions are concentrated in the inner domain, which reduces transparency. Identified zircon types are S25/S24, S18/

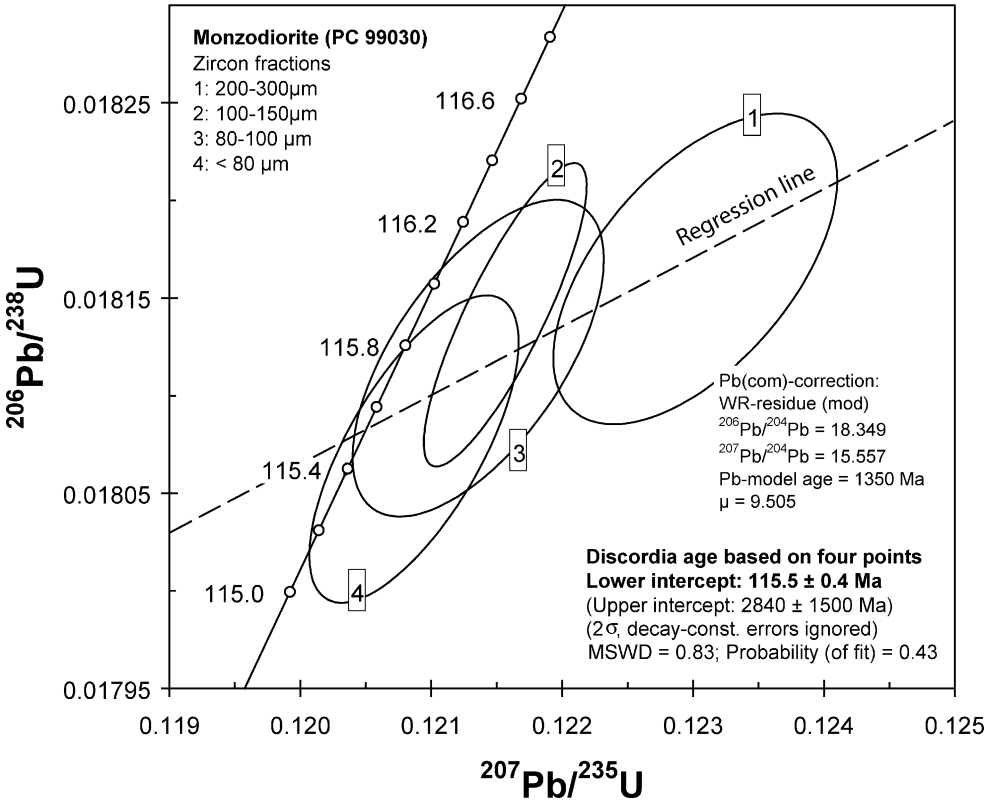

Fig. 7 U–Pb Concordia diagram of sample PC 99030 from the monzodiorite (Kmd) unit. The lower discordia intercept age (Ludwig 2001) calculated for all four fractions yields 115.5±0.4 Ma

S13, and S8/S4 (Pupin 1980, 1985). The zircons of this sample are characterized by a homogeneous outermost growth zone as observed under cathode luminescence (Fig. 3j–l). The zircons may or may not contain a medial tube (Fig. 3j) or a dark central zone (Fig. 3k) or an inherited core (Fig. 3l). A marked dark boundary zone separates an inner from the outer growth zone (Fig. 3k,l). The boundary zone has an outer dissolution surface, which is visible in almost all zircons of this sample.

Four grain-size fractions were prepared according to their transparency. Grain-size fraction 1 (60 to 100 µm) comprises transparent crystals, while fractions 2 (100 to 150 µm) and 3 (150 to 180 µm) comprise translucent crystals. Fraction 4 contains translucent, elongated prismatic S4-type zircons (100 to 125 µm). The latter are the most abundant. According to Pupin (1980), this type commonly originates from calc-alkaline series granites.

Analytical results

Uranium and thorium concentrations in zircons of the tonalite are low (U=144 to 205 ppm; Th=118 to 219 ppm). Data of fractions 1 and 2 plot nearly concordant in the Concordia diagram (Fig. 8), whereas fractions 3 and 4 deviate from the Concordia. The best fit regression line of all four data points intersects the Concordia at 110.7± 0.4 Ma (2σ; probability of fit=0.64; MSWD=0.44). Common Pb correction of data is based on the Pb isotopic analysis on whole rock residue of tonalite sample PC 97009 of Marschik et al. (2003a). The μ-value of 9.57 is below that for average active terrestrial lead (9.74, Stacey and Kramers 1975) and shifts towards the mantle value (8.35, Zartman and Doe 1981). This is consistent with the lowest measured εNd value of +4.6 for the rocks of the Copiapó plutonic complex and a Sr initial ratio of 0.7032 (Marschik et al. 2003a). Recalculated values of $^{206}Pb/^{204}Pb$=18.405 and $^{207}Pb/^{204}Pb$=15.575 (μ=9.57; 111 Ma) result in a Pb model age of about 2,414 Ma. This Pb model age is inconsistent with this upper Concordia intercept age of about 4,251 Ma, suggesting that the Pb isotope system in parts of the zircons is disturbed (see also sample 99030). As suggested above (PC 99033), we assume that the dark central zone and the medial tube have incorporated externally derived uranium and radiogenic lead. An inherited radiogenic lead component in the cores may contribute to the disturbance of the Pb isotope system.

Discussion

The new U–Pb zircon ages are interpreted as maximum crystallization ages. These ages show that dacite magmatism at about 123 Ma predates the crystallization of the nearby batholithic rocks that took place between 118±1 and 110.7±0.4 Ma (Early Cretaceous; Fig. 2). The new U–Pb zircon geochronological data are consistent with the field

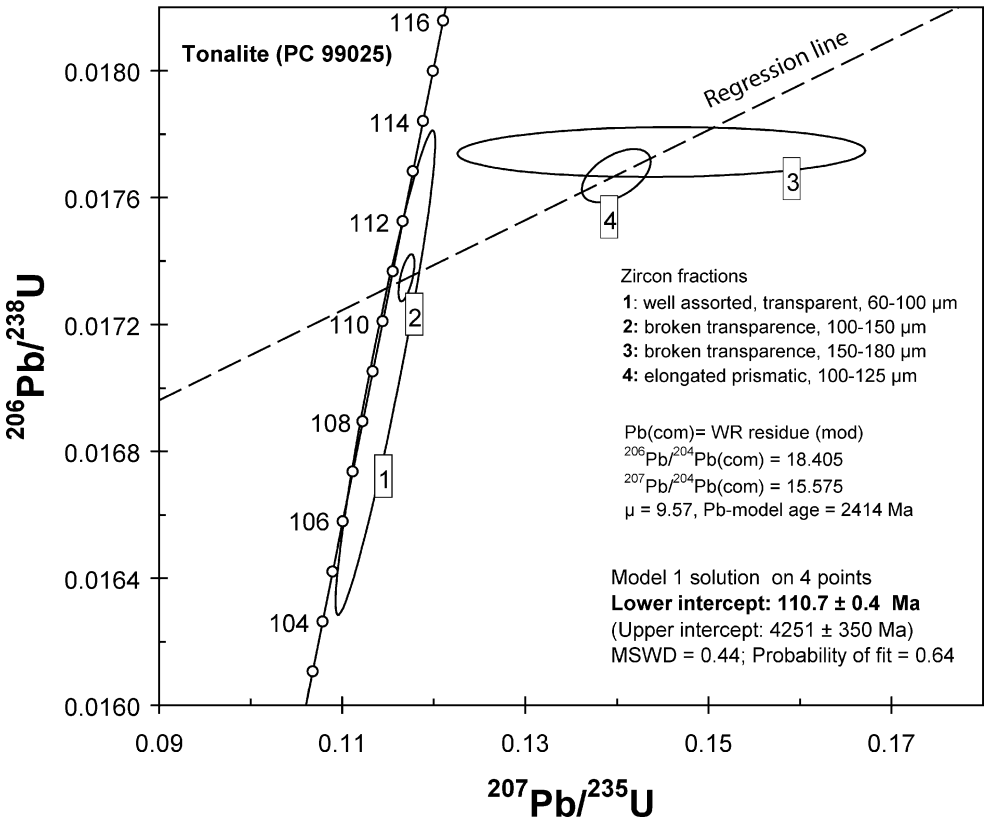

Fig. 8 U–Pb Concordia diagram of sample PC 99025 from the tonalite (Kt) unit. The regression line of all data points intersects the Concordia at 110.7±0.4 Ma and 4251± 350 Ma

relationships of the various plutons (Tilling 1962; Marschik et al. 2003a). There is a magmatic succession from hornblende diorite (118±1 Ma) via quartz monzonite (116.3±0.4 Ma) and monzodiorite (115.5±0.4 Ma) towards tonalite (110.7±0.4 Ma).

Nd model ages of the plutonic rocks range from 716 Ma (Neoproterozoic) to 488 Ma (Cambrian–Ordovician) based on a single-stage evolution model, or between 513 (middle Cambrian) to 436 (Early Silurian) based on a two-stage evolution model, respectively (Sm–Nd data from Marschik et al. 2003a). These model ages suggest a mixture of Early Cretaceous mantle and older crustal melt components. The Pb model ages vary between 160 and 2,414 Ma, also representing a mélange of ages from mantle and various crustal sources. The multigrain analysis method used provides some additional information on the provenance of the assimilated crustal Pb but does not allow identification of distinct Pb sources. We can distinguish three groups of Pb model ages: a Paleoproterozoic age of 2,414 Ma (tonalite, PC 99025), Late Paleoproterozoic–Early Mesoproterozoic ages of 1,350 Ma (monzodiorite, PC 99030) and 1,635 Ma (hornblende diorite, PC 99027), and a Jurassic age of 160 Ma (quartz–monzonite porphyry, PC 99023). There are indications of the presence of old crustal material at a depth that may have contributed Pb to the magmatic systems. Archean (2.69 to 2.78 Ga; Berg and Baumann 1985), Proterozoic (1.46 to 1.21 Ga; Damm et al. 1990), and Neoproterozoic–Cambrian (600 Ma, and 525 to 500 Ma; e.g., Berg and Baumann 1985; Lucassen et al. 2000) ages are reported. Outcrops of Carboniferous to Permian rocks occur in the Chilean Coastal Cordillera and Precordillera (e.g., Damm et al. 1981; Brown 1991; Lucassen et al. 1999). Zentilli et al. (2001) report ca. 1 Ga xenocrystic zircon in the Lower Cretaceous dacite, which hosts Cu–Au mineralization in the Punta del Cobre district and suggest that the felsic magmas picked up zircons in the Proterozoic and Paleozoic crystalline basement of the Coastal Cordillera.

Magmatism temporally overlaps with the iron oxide Cu–Au mineralization and related alteration at Candelaria–Punta del Cobre (Fig. 2). A genetic link between the mineralization and dacite porphyry dike emplacement is unlikely. The new U–Pb zircon data suggests that the dike–sill complex intruded the volcanic and metasedimentary sequence about 8 Ma before the ore formation. The question arises why the dacite is hydrothermally altered but not as heavily mineralized as the surrounding rocks. At Candelaria, the bulk of the ore is hosted by coarse volcaniclastic rocks that were porous, permeable and filled with probably connate, modified meteoric or sea waters, whereas the dacite porphyry dikes and sills are compact and dense rock masses, essentially without any permeability. Dike intrusion may have been accompanied by autometasomatism and alteration without significant associated

metallic mineralization. Potassic alteration could have occurred due to the cooling of magmatic fluids and sodic (–calcic) alteration by interaction with heating non-magmatic, saline(?) fluids stored in or drawn into the volcaniclastic rocks, respectively. The latter, ore-forming hydrothermal activity also caused alteration and locally some minor Cu–Au mineralization within the dike, but ore-forming fluids preferentially infiltrated the permeable sedimentary layers.

Marschik and Fontboté (1996) and Mathur et al. (2002) suggested that diorite magma could be related to the metallic mineralization. The age of the hornblende diorite (118±1 Ma), however, seems to preclude a genetic link. The zircon age of 116.3±0.4 Ma for the quartz–monzonite porphyry is also older than the age of the main Cu–Au mineralization (Re–Os molybdenite ages of 114.2±0.6 and 115.2±0.6 Ma; Mathur et al. 2002). However, taking a likely time delay between zircon saturation in the melt and the time of hydrothermal fluid release into account, the shoshonitic quartz–monzonite porphyry could also be responsible for the ore formation. Its porphyritic texture is consistent with rapid cooling due to sudden fluid expulsion, a fluid that could have contributed metals and sulfur. The monzodiorite (115.5±0.4 Ma) with high-K characteristics is the closest in age to the iron oxide Cu–Au mineralization at Candelaria and has the same initial $^{187}Os/^{188}Os$ within error ($^{187}Os/^{188}Os_{initial(ore)}$=0.36±0.1; $^{187}Os/^{188}Os_{initial\ (Kmd)}$= 0.27±0.02; Mathur et al. 2002). Therefore, the monzodiorite could also be responsible for the ore formation. Additionally, there are field relationships that seem to support such a hypothesis. The monzodiorite has north–northwest trending structural contacts to the east and west (Fig. 1), i.e., its emplacement was probably controlled by similar structures that controlled some of the iron oxide Cu–Au mineralization in the district (Marschik and Fontboté 1996, 2001a). Furthermore, the Candelaria mine lies to the south–southwest of the monzodiorite pluton, i.e., along strike of the structure that forms the eastern limit of the outcrop of the pluton (Fig. 1). The monzodiorite may therefore underlie the Candelaria deposit. However, these spatial configurations could also have developed through post-mineralization tectonic events. Post-mineralization block faulting may also explain why intense pervasive sodic(–calcic) alteration is not observed in the monzodiorite, whereas this alteration affected the pyroxene diorite, hornblende diorite, and quartz–monzonite porphyry, where they form the eastern margins of the batholith (Fig. 1). In addition to the pervasive sodic(–calcic) alteration, the quartz–monzonite porphyry is locally cut by numerous amphibole–scapolite bearing veins that are similar to amphibole ± scapolite-rich veins observed in the upper part of the Candelaria deposit. Voluminous sodic (–calcic) alteration is common in IOCG districts (e.g., Pollard 2001); however, its role in ore genesis remains unclear. In the case of Candelaria, the district scale sodic (–calcic) alteration developed sodic scapolite and/or albite-rich assemblages ± calcic amphibole ± pyroxene ± epidote ± andraditic or almandine-rich garnet in the sedimentary country rocks adjacent to the batholith (Marschik and Fontboté 2001a). This alteration could have occurred during contact metamorphism by heating saline waters trapped in the sedimentary rocks, which also infiltrated the plutonic rocks, and each intrusion may have triggered an own alteration cell. At Candelaria, paragenetic relationships suggest that the main sulfide mineralization postdates peak contact metamorphic assemblages and the sodic(–calcic) alteration, though these events may have also been in time. These relationships imply that at least parts of the quartz–monzonite porphyry were crystallized before the main mineralization occurred.

The younger alteration ages between 110 and 112 Ma suggest that there was hydrothermal activity that produced similar hydrothermal mineral associations as those that accompanied the main mineralization at around 115 Ma (Fig. 2).

The tonalite age (110.7±0.4 Ma) overlaps with the late alteration ages at 110 to 112 Ma. Tonalite emplacement may have driven hydrothermal cells that caused this late alteration or modified $^{40}Ar/^{39}Ar$ and K/Ar systematic in some areas. A thermal influence and modification of K/Ar ages may explain the relatively young K–Ar biotite age of 111±3 Ma for the hornblende diorite at Quebrada Las Pintadas reported by Arévalo (1994). The hornblende diorite has a direct contact with the tonalite not far from where the sample for K/Ar analysis was taken. The $^{40}Ar/^{39}Ar$ biotite-weighted mean plateau age of 109.8± 0.4 Ma (1σ) and the $^{40}Ar/^{39}Ar$ hornblende-weighted mean plateau age of 110.1±1.3 Ma (1σ) for the tonalite unit reported by Arévalo (1999) may represent unmodified cooling ages. They suggest that the crystallization and cooling below the closure temperature of hornblende and biotite may have occurred within one million years or less. This is consistent with the regional geologic context, which suggests that the plutons were emplaced at relatively shallow levels during uplift and experienced rapid post-magmatic cooling.

Conclusions

The new U–Pb zircon ages are interpreted as crystallization ages or maximum ages. They show that dacite magmatism around 123 Ma preceded the crystallization of the hornblende diorite (Khd) at 118±1 Ma, the quartz–monzonite porphyry (Kqm) at 116.3±0.4 Ma, the monzodiorite (Kmd) at 115.5±0.4 Ma, and the tonalite (Kt) at 110.7±0.4 Ma. The new geochronological data are consistent with field

relationships of the plutons. Plutonism temporally overlaps with the iron oxide Cu–Au mineralization (~115 Ma) and silicate alteration (mainly from 114 to 116 Ma and 110 to 112 Ma) at Candelaria–Punta del Cobre. Previous studies of these ore deposits suggest that the sulfur and metals are mainly derived from magmatic sources. The dacite and hornblende diorite intrusions preceded the ore formation. A genetic link of the metallic mineralization with metaluminous, high-K to shoshonitic granitoids with SiO_2 contents around 60 to 65 wt% is likely. The quartz–monzonite porphyry and/or the monzodiorite may have provided energy and contributed fluids, metals, and sulfur to the hydrothermal system that caused the mineralization in the Candelaria–Punta del Cobre district. Tonalite emplacement may have sustained existing or driven newly developed hydrothermal cells that caused late alteration at 110 to 112 Ma or modified $^{40}Ar/^{39}Ar$ and K/Ar systematic in some areas.

Acknowledgements We thank Richard A. Leveille of Phelps Dodge Exploration Corporation and Luis Alvarez L., and Walter Martin V. of Compañía Contractual Minera Candelaria for support and field assistance. The manuscript benefited from valuable suggestions by Patrick Williams, Bernd Lehmann, and an anonymous reviewer. This investigation was supported by a grant of the Deutsche Forschungsgemeinschaft to R. Marschik.

References

Arancibia G (2004) Mid-Cretaceous crustal shortening: evidence from a regional-scale ductile shear zone in the Coastal Range of central Chile. J S Am Earth Sci 17:209–226

Arévalo C (1994) Mapa Geológico del Cuadrángulo Los Loros. Scale 1:100 000. SERNAGEOMIN, Santiago, Chile

Arévalo C (1995) Mapa Geológico de la Hoja Copiapó, Región de Atacama. Santiago, Chile, SERNAGEOMIN, Scale 1:100 000

Arévalo C (1999) The Coastal Cordillera–Precordillera boundary in the Copiapó area, northern Chile and the structural setting of the Candelaria Cu–Au ore deposit. Ph.D. Thesis, Kingston University, Kingston-upon-Thames, UK, pp 1–244

Berg K, Baumann A (1985) Plutonic and metasedimentary rocks from the Coastal Range of northern Chile: Rb–Sr and U–Pb isotopic systematics. Earth Planet Sci Lett 75:101–115

Berg K, Breitkreuz C, Damm KW, Pichowiak S, Zeil W (1983) The north Chilean Coastal Range—an example for the development of an active continental margin. Geol Rundsch 72:715–731

Brown M (1991) Comparative geochemical interpretation of Permian–Triassic plutonic complexes of the Coastal Range and Altiplano (23°30′ to 26°30′S), northern Chile. Geol Soc Amer Spec Pap 265:157–171

Brown M, Diaz F, Grocott J (1993) Displacement history of the Atacama fault system 25°00′S–27°00′S, northern Chile. Geol Soc Amer Bull 105:1165–1174

Chiaradia M, Banks D, Cliff R, Marschik R, de Haller A (2006) Origin of fluids in iron oxide–copper–gold deposits: constraints from $\delta^{37}Cl$, $^{87}Sr/^{86}Sr_i$ and Cl/Br. Miner Depos 41(6):565–573

Corvalán J (1974) Estratigrafía del Neocomiano marino de la región al sur de Copiapó, Provincia de Atacama. Rev Geol Chile 1:13–36

Damm KW, Pichowiak S, Zeil W (1981) The plutonism in the North Chilean Coast-Range and its geodynamic significance. Geol Rundsch 70:1054–1076

Damm KW, Pichowiak S, Harmon RS, Todt W, Kelley S, Omarini R, Niemeyer H (1990) Pre-Mesozoic evolution of the Central Andes: the basement revisited. Geol Soc Amer Spec Pap 241:101–126

Damm KW, Harmon RS, Kelley S (1994) Some isotope and geochemical constraints on the origin and evolution of the Central Andean basement (19°–24°S). In: Reutter KJ, Scheuber E, Wigger PJ (eds) Tectonics of the Southern Central Andes. Springer, Berlin Heidelberg New York, pp 263–275

Farrar E, Clark AH, Haynes SJ, Quirt SG, Conn H, Zentilli M (1970) K–Ar evidence for the post Paleozoic migration of granitic intrusion foci in the Andes of Northern Chile. Earth Planet Sci Lett 10:60–66

Friedman I, O'Neil JR (1977) Compilation of stable isotope fractionation factors of geochemical interest. In: Fleischer M (ed) Data of geochemistry. US Geological Survey Professional Paper 440-KK, p 12

Gana P, Zentilli M (2000) Historia termal y exhumación de intrusivos de la Cordillera de la Costa de Chile central. 9. Congreso Geológico Chileno, Puerto Varas pp 664–668

Geisler T, Pidgeon RT, van Bronswijk W, Kurtz R (2002) Transport of uranium, thorium, and lead in metamict zircon under low-temperature hydrothermal conditions. Chem Geol 191:141–154

Gradstein FM, Agterberg FP, Ogg JG, Hardenbol J, Van Veen P, Thierry J, Huang Z (1995) A Triassic, Jurassic and Cretaceous time scale. In: Berggren WA, Kent DV, Aubry MP, Hardenbol J (eds) Geochronology, time scales and global stratigraphic correlation. Society for Sedimentary Geology 54:95–126

Grocott J, Wilson J (1997) Ascent and emplacement of granitic plutonic complexes in subduction-related extensional environments. In: Holness M (ed) Deformation enhanced melt segregation and metamorphic fluid transport. Miner Soc Ser environments 7:173–192

Grocott J, Brown M, Dallmeyer RD, Taylor GK, Treloar PJ (1994) Mechanism of continental growth in extensional arcs: an example from the Andean plate-boundary zone. Geology 22:391–394

Jurgan H (1977a) Zur Gliederung der Unterkreide-Serien in der Provinz Atacama, Chile. Geol Rundsch 66:404–434

Jurgan H (1977b) Strukturelle und lithofazielle Entwicklung des andinen Unterkreide-Beckens im Norden Chiles (Provinz Atacama). Geotekton Forsch 52:1–138

Krogh TE (1973) A low-contamination method for hydrothermal decomposition of zircon and extraction of U and Pb for isotope age determination. Geochim Cosmochim Acta 37:485–494

Krogh TE (1982) Improved accuracy of U–Pbzircon ages by the creation of more concordant systems using an air abrasion technique. Geochim Cosmochim Acta 46:637–649

Lucassen F, Franz G, Thirlwall MF, Mezger K (1999) Crustal recycling of metamorphic basement: Late Paleozoic granites of the Chilean Coast Range and Precordillera at−22°S. J Petrol 40:1527–1551

Lucassen F, Becchio R, Wilke HG, Franz G, Thirlwall MF, Viramonte J, Wemmer K (2000) Proterozoic–Paleozoic development of the basement of the Central Andes (18–26°S)—a mobile belt of the South American craton. J S Am Earth Sci 13:697–715

Lucassen F, Harmon R, Franz G, Romer RL, Becchio R, Siebel W (2002) Lead evolution of the Pre-Mesozoic crust in the Central Andes (18–27°): progressive homogenisation of Pb. Chem Geol 186:183–197

Ludwig KR (1993) PBDAT—A computer program for processing Pb–U–Th isotope data (version 1.24). US Geological Survey Open File Report 88-542, p 34

Ludwig KR (2001) Users manual for Isoplot/Ex rev. 2.49: a geochronological toolkit for Microsoft Excel. Berkeley Geochronology Center, Special Publication 1a. Berkeley, CA, USA, p 55

Marschik R, Fontboté L (1996) Copper(–iron) mineralization and superposition of alteration events in the Punta del Cobre belt, northern Chile. In: Camus F, Sillitoe RM, Petersen R, Sheahan P (eds) Andean copper deposits: new discoveries, mineralization, styles and metallogeny. Economic Geology Special Publication no. 5, pp 171–189

Marschik R, Fontboté L (2001a) The Candelaria–Punta del Cobre iron oxide Cu–Au(–Zn–Ag) deposits, Chile. Econ Geol 96:1799–1826

Marschik R, Fontboté L (2001b) The Punta del Cobre formation, Punta del Cobre–Candelaria area, northern Chile. J S Am Earth Sci 14:401–433

Marschik R, Singer BS, Munizaga F, Tassinari C, Moritz R, Fontboté L (1997) Age of Cu(–Fe)–Au mineralization and thermal evolution of the Punta del Cobre district, Chile. Miner Depos 32:531–546

Marschik R, Leveille RA, Martin W (2000) La Candelaria and the Punta del Cobre district, Chile: Early Cretaceous iron oxide Cu–Au(–Zn–Ag) mineralization. In: Porter TM (ed) Hydrothermal iron–oxide copper–gold & related deposits: a global perspective. Australian Mineral Foundation, Adelaide, pp 163–175

Marschik R, Fontignie, D, Chiaradia M, Voldet P (2003a) Geochemical and Nd–Sr–Pb–O isotope characteristics of granitoids of the Early Cretaceous Copiapó plutonic complex (27°30'S), Chile. J S Am Earth Sci 16:381–398

Marschik R, Chiaradia M, Fontboté L (2003b) Implications of Pb isotope signatures of rocks and iron oxide Cu–Au ores in the Candelaria–Punta del Cobre district, Chile. Miner Depos 38:900–912

Mathur R, Marschik R, Ruiz J, Munizaga F, Leveille RA, Martin W (2002) Age of mineralization of the Candelaria iron oxide Cu–Au deposit, and the origin of the Chilean Iron Belt based on Re–Os isotopes. Econ Geol 97:59–71

McNutt RH, Crockett JH, Clark AH, Caelles JC, Farrar E, Haynes SJ, Zentilli M (1975) Initial $^{87}Sr/^{86}Sr$ ratios of plutonic and volcanic rocks of the Central Andes between latitudes 26°–29°S. Earth Planet Sci Lett 27:303–313

McNutt RH, Clark AH, Zentilli M (1979) Lead isotope compositions of Andean igneous rocks, latitudes 26°–29°S: Petrologic and metallogenic implications. Econ Geol 74:827–837

Mezger K, Krogstad EJ (1997) Interpretation of discordant U–Pb zircon ages: an evaluation. J Metamorph Geol 15:127–140

Ministry of Mines, Chile (2002) Explore Chile: a world leader in mining. Northern Miner, pp 1–8 (advertising supplement)

Mourgues FA (2004) Advances in ammonite biostratigraphy of the marine Atacama basin (Lower Cretaceous), northern Chile, and its relationship with the Neuquén basin, Argentina. J S Am Earth Sci 17:3–10

Pollard PJ (2001) Sodic(–calcic) alteration in Fe–oxide–Cu–Au districts: an origin via unmixing of magmatic H_2O–CO_2–NaCl±$CaCl_2$–KCl fluids. Miner Depos 36:93–100

Pupin JP (1980) Zircon and granite petrology. Contrib Mineral Petrol 73:207–220

Pupin JP (1985) Magmatic zoning of Hercynian granitoids in France based on zircon typology. Schweiz Mineral Petrogr Mitt 65:29–56

Rabbia OM, Frutos J, Pop N, Isache C, Sanhueza V, Edelstein O (1996) Características isotópicas de la mineralización de Cu(–Fe) de Mina Carola, distrito minero Punta del Cobre, norte de Chile. Congr Geol Argentino, 8th, Actas, 1996, Buenos Aires 3:241–254

Scheuber E, Andriessen PAM (1990) The kinematic and geodynamic significance of the Atacama fault zone, northern Chile. J Struct Geol 12:243–257

Scheuber E, Hammerschmidt K, Friedrichsen H (1995) $^{40}Ar/^{39}Ar$ and Rb–Sr analyses from ductile shear zones from the Atacama Fault Zone, Northern Chile: the age of deformation. Tectonophysics 250:61–87

Segerstrom K, Parker RL (1959) Geología del cuadrángulo Cerrillos, Provincia de Atacama. Carta Geológica de Chile 13, SERNA GEOMIN, Santiago, Chile p 50

Sommerauer J (1976) Trace element distribution patterns and the mineralogical stability of zircon—an application for combined electron probe techniques. Proc Electron Microscopy Soc Southern Africa 4:71–72

Stacey JS, Kramers JD (1975) Approximation of terrestrial lead isotope evolution by a two-stage model. Earth Planet Sci Lett 26:207–221

Steiger RH, Jäger E (1977) Subcommision on geochronology: convention on the use of decay constants in geo- and cosmochronology. Earth Planet Sci Lett 36:359–362

Tilling R (1962) Batholith emplacement and contact metamorphism in the Paipote-Tierra Amarilla area, Atacama Province, Chile. Ph.D. Thesis. Yale University, New Haven, CT, USA, p 195

Tilling R (1963a) Batholith emplacement and contact metamorphism near Tierra Amarilla, Atacama province, Chile (abstract). Geol Soc Amer Spec Pap 76:166–167

Tilling R (1963b) Disequilibrium skarns of the Tierra Amarilla aureole, Atacama province, Chile (abstract). Geol Soc Amer Spec Pap 76:167

Tilling R (1976) El Batolito Andino cerca de Copiapó, Provincía de Atacama. Geología y Petrología. Rev Geol Chile 3:1–24

Ullrich T, Clark AH (1999) The Candelaria copper–gold deposit, región III, Chile: paragenesis, geochronology and fluid composition. In: Criddle AJ, Hagni RD (eds) Mineral deposits: processes to processing. Balkema, Rotterdam, pp 201–204

Ullrich TD, Clark AH, Kyser TK (2001) The Candelaria Cu–Au deposit, III region, Chile: product of long-term mixing of magmatic–hydrothermal and evaporite-sourced fluids. In: Geological Society of America Annual Meeting, Boston, MA, Abstract Programs, p A-3

Zartman RE, Doe BR (1981) Plumbotectonics. The model. Tectonophysics 75:135–162

Zentilli M (1974) Geological evolution and metallogenetic relationships in the Andes of northern Chile between 26° and 29°S. PhD Thesis, Queen's University, Kingston, Ontario, pp 1–394

Zentilli M, Pop N, Heaman L, Boric R (2001) Evidence of Proterozoic crust under the Coastal Cordillera of Central Chile: Grenville age xenocrystic zircons in Cretaceous volcanic rocks. III. South American Symposium on Isotope Geology, Pucon, Chile, p 642